



## Rationale for the crystallization of titania polymorphs in solution

Journal:	<i>Nanoscale</i>
Manuscript ID:	NR-ART-07-2014-004346.R1
Article Type:	Paper
Date Submitted by the Author:	16-Sep-2014
Complete List of Authors:	Kraenzlin, Niklaus; ETH Zurich, Department of Materials Staniuk, Malwina; ETH Zurich, Department of Materials Heiligtag, Florian; ETH Zurich, Department of Materials Luo, Li; ETH Zurich, Department of Materials Emerich, Hermann; Swiss Norwegian Beamlines (SNBL), van Beek, Wouter; SNBL, Niederberger, Markus; ETH Zurich, Department of Materials Koziej, Dorota; ETH Zurich, Department of Materials

## Rationale for the crystallization of titania polymorphs in solution

N. Kränzlin,<sup>a</sup> M. Staniuk,<sup>a</sup> F. J. Heiligtag,<sup>a</sup> L. Luo,<sup>a</sup> H. Emerich,<sup>b</sup> W. van Beek,<sup>b</sup> M. Niederberger,<sup>a</sup> and D. Koziej<sup>a\*</sup>

<sup>a</sup> Laboratory for Multifunctional Materials, Department of Materials, ETH Zürich, Vladimir-Prelog-Weg 5, 8093 Zürich, Switzerland

<sup>b</sup> Swiss-Norwegian Beamlines at European Synchrotron Research Facility, 6 Rue Jules Horowitz, 38043 Grenoble, France

\* Corresponding author: dorota.koziej@mat.ethz.ch

### Abstract

We use in-situ X-ray absorption and diffraction studies to directly monitor the crystallization of different titania polymorphs in one and the same solution. We find that despite of commonly accepted polymorphic-crossover from anatase to rutile triggered by the critical size of nanoparticles, in the solution their respective nucleation and growth are independent processes. Moreover, we find that 5.9 nm rutile nanoparticles are formed prior to the formation of 8.4 nm anatase nanoparticles. Our results suggest that the origins of this crystallization mechanism are the formation of an intermediate non-crystalline phase and time dependent changes of the chemical environment.

### Introduction

Polymorphism, the occurrence of different structures with the same composition, is interesting for a variety of applications ranging from biomaterials, pharmaceuticals to materials commonly used in the energy-related applications. Understanding and controlling the formation of different polymorphs is a key to fascinating discoveries. For example the  $\alpha$ -polymorph of  $\text{LiFePO}_4$ , in contrast to its  $\beta$ -polymorph, allows achieving an excellent electrochemical performance of Li-ion batteries.<sup>1</sup> A showcase example for taking advantages of polymorphism provides carbon; its diamond, graphite, and graphene structures open up an overwhelmingly broad field of applications.<sup>2</sup> For titania ( $\text{TiO}_2$ ), the two most prominent polymorphs, besides the less common brookite and other artificial modifications, are anatase and rutile. Driven by the perpetual optimization of photo-catalysts operating in the visible light range, surface specific chemical activity effects,<sup>3-9</sup> synergistic properties resulting from combining the different electronic band configurations of anatase and rutile phase,<sup>8, 10-14</sup> meso-structuring strategies<sup>15-22</sup> and others<sup>8, 23-26</sup> have been investigated in detail and were identified as being responsible for high photo-catalytic efficiency. Application-oriented usage of  $\text{TiO}_2$  and its polymorphs is by far not limited to the field

of photo-catalysis or photo-voltaics, where the anatase phase generally is preferred. Rutile-TiO<sub>2</sub> exhibits a high refractive index, light scattering efficiency and UV absorptivity.<sup>27-28</sup> Therefore rutile powder finds direct use as UV-filter in sunscreens, pigments in paintings and filler material in cosmetic products. More sophisticated technologies take advantage of the very same properties of titania in coatings of self-cleaning surfaces and smart windows.<sup>29</sup> Irrespective of the particular application the usable property on the macroscopic scale is the outcome of a complex interplay of the particles' phase, size, morphology, surface/surface chemistry and crystallinity. These factors are a characteristic of the specific synthetic strategy employed.<sup>3</sup> In particular wet-chemical routines have proven their exceptional versatility in gaining control over evolving nano-phases, their morphology and size<sup>30</sup> but it remains unclear, why a specific polymorph or polymorph mixture forms under given reaction conditions.<sup>31</sup> Assuming thermodynamic equilibrium conditions, free surface energy calculations on the different facets of anatase and rutile and measurements of surface enthalpies, readily provide an explanation. Below a critical particle size ( $d_{\text{crit}}$ ) the anatase modification is energetically more stable than the rutile configuration of TiO<sub>2</sub>.<sup>32</sup> Several authors experimentally confirmed these findings by heat-treating anatase nanocrystals, and a value often reported is  $d_{\text{crit}} \approx 14$  nm.<sup>33-36</sup> Consequently, the synthesis of nanosized rutile TiO<sub>2</sub> necessitates systems, where thermodynamic equilibration is not dictating nucleation, coarsening and aggregation of the evolving TiO<sub>2</sub> crystals. Such systems are typically represented by liquid phase syntheses, where for example strongly binding species drastically reduce the surface energy ( $\gamma$ ) of individual facets<sup>5-6</sup> and influence the evolving phase, size and morphology of the corresponding crystals. States far from thermodynamic equilibrium are predominant. In general, it is believed that slower crystallization will lead to rutile, and rapid crystallization favors anatase formation.<sup>37</sup> This reasoning is often used in explaining both the stability of anatase nanocrystals and the difficulties in synthesizing rutile nanocrystals smaller than 14 nm by wet-chemical routes. Reported strategies that prepare nano-sized rutile TiO<sub>2</sub> relate their success to the high acidic environment,<sup>38-39</sup> high temperature<sup>40-41</sup> or high pressure<sup>40</sup> in which crystallization proceeds. However, so far there are no experimental reports on in-situ monitoring of phase-crossover from anatase to rutile in solution, as would be expected from kinetically controlled cascade crystallization from less dense to more dense phases.<sup>42</sup> Furthermore, recently rutile nanocrystals slightly smaller than crossover size were synthesized directly from the solution.<sup>31</sup> Thus, studying such systems that do not necessarily obey paradigms postulated by classical nucleation theory is essential to rationalize nanocrystals synthesis in solution and to lay the foundation for precise description of crystallization in a chemically active environment.

Here, we select the synthesis approach reported by Yu Wu et al.<sup>38</sup> because it features the necessary characteristics for the phase pure preparation of both TiO<sub>2</sub> polymorphs by reacting titanium tetrachloride (TiCl<sub>4</sub>) with acetone. We use in situ powder X-ray diffraction (PXRD) and X-ray absorption spectroscopy (XAS) to follow the time dependent genesis of (non-)crystalline intermediates and titania polymorphs in solution. In our focus are processes preceding nucleation and dependencies between anatase and rutile formation in solution. This is possible, because both polymorphs are consecutively formed in the same reaction solution under isothermal conditions at 120 °C.

## Experimental

*Chemicals.* Titanium tetrachloride (TiCl<sub>4</sub>, Sigma-Aldrich 99.9%) was used as precursor and acetone (Sigma-Aldrich, ≥ 99.9%) served as solvent.

*Synthesis.* TiCl<sub>4</sub> was added to acetone (molar ratio 1:5) under vigorous stirring in ambient conditions. The reaction solution turned slightly yellowish but still remained transparent. No precipitation could be observed at this stage and the vigorous stirring guaranteed a homogenous mixing/dissolution throughout the sample volume. Stirring was maintained for 5 min. (a) For the experiment under laboratory conditions, 15 ml of the as prepared reaction solution was transferred into a 45 ml Teflon liner, sealed in a Paar acid digestion bomb and placed in an oven for 6 and 12 hours at 120 °C. After cooling down, the precipitate was centrifuged, washed with ethanol and the resulting powder was dried in an oven at 60 °C. (b) For the in-situ experiments, 1 mL of the as prepared solution was then transferred into the measurement cell, which was tightly sealed and aligned to let the beam pass through the sample volume at a centric position (see Figure S1). After the alignment procedure precipitation of large transparent crystals was observed. From this point on, no changes were made which could affect the irradiated volume of the sample assuring constant volume conditions throughout all the following in-situ PXRD and XAS measurements. The only possible source of fluctuations refers to particle size/mass dependent sedimentation effects, as the solution was not stirred during the time of reaction. The adjustment of the current flowing through the resistive heating elements of the cell allowed for homogeneously heating the sample volume to 120 °C. Once the temperature reached 120 °C all the parameters were kept constant until the end of the experiment.

*Synchrotron-based studies.* The experiments were performed at the European Synchrotron Radiation Facility (ESRF), Grenoble at the Swiss Norwegian Beamlines (SNBL). The in-situ experiment lasted in total for 67 hours and can be divided in four distinct stages as shown in Figure S1. We define the acquisitions loops for each stage separately, which allows us to follow the dynamic changes of crystalline and non-crystalline species and to optimize the information

content. Further experimental details, set-up, recorded raw data and data handling procedures are given in the electronic supporting information.

### Results and discussion

Already at room temperature we observe precipitation of large transparent crystals inside the initially transparent reaction solution. Interestingly, indexing of the corresponding PXRD pattern in Figure 1A and Figure S3 disclosed a single monoclinic phase of  $\text{Ti}(\text{OH})_x\text{Cl}_{4-x}$ .<sup>38</sup> From the Fourier Transform of the extended X-ray absorption fine structure (EXAFS) spectrum the average distance to the first coordination sphere of Ti is determined to be 1.8 Å. Heating the reaction solution to 120 °C induces dissolution of the initially formed  $\text{Ti}(\text{OH})_x\text{Cl}_{4-x}$  crystals, which is manifested by the gradual disappearance of all diffraction peaks. Moreover, the radial distribution function reveals a successive decrease of the distance between the titanium ions and their first coordination sphere from 1.8 Å to 1.35 Å, as shown in Figure 1B. The values do not represent the absolute Ti-O,Cl distances in the structures, because the data are not corrected for the backscattering phase shift. But the relative change of 0.45 Å is significant. Additionally X-ray absorption near edge structure (XANES) spectra show upshifting of the whiteline of about 0.8 eV and development of pre-edge peaks A1-A3 characteristic for titania,<sup>43</sup> Figure 1C. These results confirm the formation of Ti containing compounds lacking long-range periodic order. This process of transformation is assumed to follow crystal dissolution kinetics, which could be described by deceleratory sigmoidal conversion.<sup>44</sup> Here, dissolving has to be understood as a transformation into non-crystalline intermediate species. No information on the size of the non-crystalline species can be extracted from the recorded data. It takes 400 minutes until we observe the first diffraction peak. Strikingly, this peak corresponds to the lattice spacing of the (110) planes of the tetragonal rutile modification of  $\text{TiO}_2$  as shown in Figure 2A. The FWHM value of the (110) peak scatters in the beginning but stabilizes after 700 min around  $0.439 \pm 0.049$  as shown in Figure 2F. Together with the time dependent change of the absolute peak intensity of the (110) reflection shown in Figure 2G it can be concluded that rutile particles nucleate and grow to a size of 5.9 nm and their phase amount approaches a saturation level.

Later in time the reflection corresponding to the d-spacing of the (101) planes of anatase  $\text{TiO}_2$  appears. Interestingly the FWHM values also remain constant around  $0.309 \pm 0.013$  as shown in Figure 2F. The evolution of the absolute peak intensity of the (101) reflection increases like in the case of rutile crystals as shown in Figure 2G. Anatase nanocrystals nucleate and grow to a constant size of 8.4 nm with the phase amount also approaching a saturation level. These findings directly prove that indeed, in the as-described solute system, no crossover-size triggers the crystallization of titania polymorphs.

In general, modification of the sample due to interactions with the X-ray beam is assumed to be negligible. However, the extended exposure for several hours, as in our experiment, may lead to: (a) local heating due to X-ray absorption, (b) structural changes due to the kinetic energy of photoelectrons, created by absorption of the X-rays and (c) structural changes due to absorption of X-rays that have been previously scattered.<sup>45</sup> For titania nanocrystals, it has been recently shown that an exposure to X-rays causes a slight reduction of  $Ti^{4+}$  at the surface.<sup>46</sup> However, no references are available on the impact of X-rays on nucleation and growth of titania nanocrystals in solution at elevated temperatures. Thus, to prove that the hereby-described reaction is independent of the X-ray irradiation we perform a control experiment under laboratory conditions. If we stop the reaction after 6 hours, we observe in the XRD pattern only the reflection corresponding to 6 nm large rutile nanocrystals, whereas after 12 hours we observed both polymorphs anatase and rutile as shown in Figure S9. The consecutive formation of rutile and anatase resemble closely the findings from the in-situ experiments. Therefore we can clearly exclude an influence of the X-ray irradiation on the mechanism of titania polymorphs formation.

Moreover we extract further information on the two titania polymorphs in solution from the full pattern refinement of the PXRD records as shown in Figure S4. Compared to the double peak fitted results a very slight trend towards smaller FWHM values with increasing reaction time can be identified shown in Figure 2F. The scale factors output from the full pattern fits further support the existence of phase equilibrium towards the end of reaction time as shown in Figure 2G.

To complete the picture, all the size information accessible by refinement of the long range recorded PXRD data is compared to the critical particle size for anatase to rutile phase transformation as it is reported from studies on the thermal treatment of anatase nanocrystals.<sup>33-36, 47</sup> As the critical particle size has to be interpreted as an average particle size disregarding morphological anisotropy effects, its graphical representation is a sphere with a diameter of 14 nm. The refined PXRD patterns reveal directional size information on nanocrystals based on the widening of all indexed reflections. Their contoured orthogonal projection on a,b a,c and b,c planes at different reaction times are shown in SI Figure S5-S6. The comparison of the initial and final shapes of anatase and rutile nanocrystals are shown in Figure 2B and C, respectively. The calculated shapes help clarifying how anisotropy affects the extracted nanocrystals size. However, they are not intended to reveal the crystallites' actual shapes as the spatial expansion can only be calculated in directions perpendicular to lattice planes which give rise to Bragg peaks in the diffractograms.

The graphical comparison between the formed  $TiO_2$  nanocrystals and the critical particle size is realized by superimposing a sphere with diameter of 14 nm to all the directional sizes of both

anatase and rutile. After 1420 min both polymorphs exhibit certain degree of anisotropy but all directional sizes stay well below the critical crossover size of 14 nm as shown in Figure 2D. Towards the end of the reaction the rutile crystallites tend to marginally grow and increase the degree of anisotropy whereas the anatase crystallites just slightly grow as shown in Figure 2E. Most importantly the data show the coexistence of rutile and anatase nanocrystals at a size smaller than 14 nm and their independent size evolution with time of reaction.

The rationale for titania polymorph crystallization in solution can be given based on the aforementioned experimental findings as it is schematically shown in Figure 3A. In contrast to classical nucleation theory or predictions of the equilibrium structure of crystals from free surface energy calculations,<sup>34</sup> we assume that the initially high acidity of the reaction solution accompanied by a high  $\text{Cl}^-$  concentration triggers the formation of rutile in a first step. With time, different condensation reactions<sup>38</sup> change the chemical composition of the solution mainly by formation of  $\text{H}_2\text{O}$  allowing the  $\text{Cl}^-$  to volatilize as  $\text{HCl}$ , decreasing the acidity of the solution and  $\text{Cl}^-$  concentration in the course of reaction finally favoring the crystallization of anatase.

Different theoretical scenarios for the anatase formation are schematically depicted in Figure 3 as V1-V4. In V2 it was assumed that rutile is undergoing a solid phase transformation to anatase with time of reaction. This would mean that the rutile phase should both show a decrease in its average size and also phase amount with time; meanwhile, the anatase should show the opposite behavior. Figure 2F and 2G clearly show contradictory trends. In V4 the formed rutile phase dissolves with time and anatase crystallizes out of solution, which would give similar trends from PXRD pattern evaluation as discussed in the case of V2. Again this is not observed here. Possible scenarios, which fit the trends extracted from the recorded PXRD patterns, are schematically represented in V1 and V3. The Ti containing compound, lacking in long-range periodic order shown in Figure 3, stage III is partially consumed during the initial crystallization of rutile. The later formation of anatase crystals originates likewise from the same species in the solution triggered by the changed chemical environment.

We finally prove this hypothesis by applying the MCR-ALS method to determine the number of chemical species in the solution from XANES data. We use the SIMPLISMA algorithm, which is a variance-based method, to find the initial spectra of the components, whose concentration significantly differ from scan to scan as compared to other components.<sup>48-51</sup> Further details about the MCR-ALS method are given in the Supporting Information. We find three independent components and their spectra, as shown in Figure 4. The spectrum of component 1 shows initially formed crystalline  $\text{Ti}(\text{OH})_x\text{Cl}_{4-x}$  species before dissolution. The pre-edge area of spectrum 2 and 3 look rather similar. However, in the post-edge area, spectrum 3 in comparison to spectrum 2

shows significantly more pronounced features. These features arise from X-ray scattering on atoms that occupy specified positions and its more pronounced intensities reveal an increasing average number of scatterers surrounding the central atom.<sup>52-54</sup> Meanwhile the component number 1 dissolves, component number 2, lacking long-range periodic order, forms equivalently. After approximately 150 minutes we observe ordering in the solution, which is attributed to the formation of component number 3. This is before the detection of any crystalline nanoparticles by PXRD. These findings further support the formation of an intermediate phase prior to rutile or anatase nucleation. Since no information is available on the size of this intermediate phase we do not differentiate between non-crystalline network-like species,<sup>38, 55</sup> pre-nucleation cluster (PNC) formation<sup>56-57</sup> or amorphous nanoparticles.

A model describing nucleation events by acceleratory phase fraction – time transients unfolds the general time dependency of the involved activation energy  $E_a$  as given by Equations 1 and 2:

$$x = e^{-\frac{\alpha}{t}} [e^{(\beta t^2)} - 1] \quad (\text{Equation 1})$$

$$E_a = E_a^0 - RT\beta t^2 \quad (\text{Equation 2})$$

where  $\alpha$  and  $\beta$  are fit parameters,  $E_a^0$  represents the time-independent portion of the activation energy,  $R$  the ideal gas constant and  $T$  the absolute temperature,  $x$  represents the fraction of intermediate phase remaining in the system at time  $t$ .<sup>44</sup> No data from temperature dependent experiments is available. Therefore, the postulated model is based on assumed values for the activation energies and it used to further consolidates the interpretation of the experimental findings.

In our reaction at 120 °C, the activation energy of rutile ( $E_{a,rutile}$ ) and anatase ( $E_{a,anatase}$ ) formation are not constant but due to the intrinsically changing chemical environment, they are also time-dependent. After the dissolution of the  $Ti(OH)_xCl_{4-x}$  phase (t1) the activation energy for establishing corner connectivity between  $TiO_6$  octahedra is lower than for sharing edges, favoring the nucleation and growth of rutile. Thus, initially at 120 °C,  $E_{a,rutile}$  is lower than  $E_{a,anatase}$  leading to the nucleation and growth of rutile  $TiO_2$ . With time the  $E_{a,rutile}$  is decreasing, accelerating the conversion of intermediate non-crystalline phase to the rutile configuration of  $TiO_2$ . After approximately 1000 min (t2) the situation reverses and  $E_{a,anatase}$  is lower than  $E_{a,rutile}$  resulting in the formation of  $TiO_2$  in the anatase configuration. The graphical representation of the activation energies and the overall degree of intermediate non-crystalline phase conversion as a function of time is qualitatively depicted in Figure 3B-C.

## Conclusions

In closing, the collected data revealed insights into a complex crystallization mechanism in a macroscopically simple system. The time dependent changes in the chemical environment directly trigger the activation energies ( $E_a$ ) involved in the nucleation of either rutile or anatase  $\text{TiO}_2$ . Further, the results show that thermodynamic equilibration does not determine nucleation and growth of the  $\text{TiO}_2$  crystals, as the rutile phase forms first, and in the beginning also at smaller sizes than anatase. So, the crossover size  $d_{\text{crit}}$  for a size induced phase transformation indeed is not an inherent material property of  $\text{TiO}_2$  but strongly depends on environmental variables.

### Notes and references

**Electronic Supplementary Information** (ESI) available: detailed instructions on the experimental part including set-up, recorded XAS and PXRD raw data and their detailed.

### Acknowledgements

The work was funded by the Swiss National Science Foundation (200021\_137637 and 200021\_140581) and ETH Zurich (ETH-05-12-2). We thank European Research Synchrotron Facility and SNBLs for beam time allocation, Gopinathan Sankar UC London for making an in-situ cell available.

- 1 G. Zeng, R. Caputo, D. Carriazo, L. Luo and M. Niederberger, *Chem. Mater.*, 2013, **25**, 3399.
- 2 A. K. Geim, *Science*, 2009, **324**, 1530.
- 3 W.-J. Ong, L.-L. Tan, S.-P. Chai, S.-T. Yong and A. R. Mohamed, *Nanoscale*, 2014, **6**, 1946.
- 4 Y. Zhao, Y. Zhang, H. Liu, H. Ji, W. Ma, C. Chen, H. Zhu and J. Zhao, *Chem. Mater.*, 2013, **26**, 1014.
- 5 M. Dozzi and E. Selli, *Catalysts*, 2013, **3**, 455.
- 6 H. G. Yang, C. H. Sun, S. Z. Qiao, J. Zou, G. Liu, S. C. Smith, H. M. Cheng and G. Q. Lu, *Nature*, 2008, **453**, 638.
- 7 A. S. Barnard and L. A. Curtiss, *Nano Lett.*, 2005, **5**, 1261.
- 8 G. Liu, L. Wang, H. G. Yang, H.-M. Cheng and G. Q. Lu, *J. Mater. Chem.*, 2010, **20**, 831.
- 9 Z. Lai, F. Peng, H. Wang, H. Yu, S. Zhang and H. Zhao, *J. Mater. Chem. A*, 2013, **1**, 4182.
- 10 T. Kawahara, Y. Konishi, H. Tada, N. Tohge, J. Nishii and S. Ito, *Angew. Chem., Int. Ed.*, 2002, **41**, 2811.
- 11 J. Zhang, Q. Xu, Z. Feng, M. Li and C. Li, *Angew. Chem., Int. Ed.*, 2008, **47**, 1766.
- 12 R. I. Bickley, T. Gonzalez-Carreno, J. S. Lees, L. Palmisano and R. J. D. Tilley, *J. Solid State Chem.*, 1991, **92**, 178.
- 13 D. C. Hurum, A. G. Agrios, K. A. Gray, T. Rajh and M. C. Thurnauer, *J. Phys. Chem. B*, 2003, **107**, 4545.
- 14 D. C. Hurum, K. A. Gray, T. Rajh and M. C. Thurnauer, *J. Phys. Chem. B*, 2004, **109**, 977.
- 15 L. Malfatti, P. Falcaro, H. Amenitsch, S. Caramori, R. Argazzi, C. A. Bignozzi, S. Enzo, M. Maggini and P. Innocenzi, *Microporous Mesoporous Mater.*, 2006, **88**, 304.
- 16 W. Cheng, W. Li, S. Ji, D. Yang, L. Wang, X. Qu, C. Zhang, F. Liang, Q. Wang, J. Li and Z. Yang, *J. Mater. Chem. A*, 2013, **1**, 8023.
- 17 D. Feng, W. Luo, J. Zhang, M. Xu, R. Zhang, H. Wu, Y. Lv, A. M. Asiri, S. B. Khan, M. M. Rahman, G. Zheng and D. Zhao, *J. Mater. Chem. A*, 2013, **1**, 1591.
- 18 F. Bosc, A. Ayrat, N. Keller and V. Keller, *J. Sol. Energy Eng.*, 2008, **130**, 041006.

- 19 T. A. Arun, D. K. Chacko, A. A. Madhavan, T. G. Deepak, G. S. Anjusree, T. Sara, S. Ramakrishna, S. V. Nair and A. S. Nair, *Rsc Advances*, 2014, **4**, 1421.
- 20 E. Nilsson, Y. Sakamoto and A. E. C. Palmqvist, *Chem. Mater.*, 2011, **23**, 2781.
- 21 G. K. Mor, K. Shankar, M. Paulose, O. K. Varghese and C. A. Grimes, *Nano Lett.*, 2005, **6**, 215.
- 22 A. S. Nair, Y. Shengyuan, Z. Peining and S. Ramakrishna, *Chem. Commun.*, 2010, **46**, 7421.
- 23 A. A. Ismail and D. W. Bahnemann, *J. Phys. Chem. C*, 2011, **115**, 5784.
- 24 A. Primo, A. Corma and H. Garcia, *Phys. Chem. Chem. Phys.*, 2011, **13**, 886.
- 25 J. Choi, H. Park and M. R. Hoffmann, *J. Phys. Chem. C*, 2009, **114**, 783.
- 26 R. Asahi, T. Morikawa, T. Ohwaki, K. Aoki and Y. Taga, *Science*, 2001, **293**, 269.
- 27 S. G. Kumar and K. S. R. K. Rao, *Nanoscale*, 2014, DOI: 10.1039/c4nr01657b.
- 28 D. Koziej, F. Fischer, N. Kränzlin, W. R. Caseri and M. Niederberger, *ACS Appl. Mater. Interfaces*, 2009, **1**, 1097.
- 29 M. Cargnello, T. R. Gordon and C. B. Murray, *Chem. Rev.*, 2014, DOI: 10.1021/cr500170p.
- 30 D. Koziej, A. Lauria and M. Niederberger, *Adv. Mater.*, 2014, **26**, 235.
- 31 A. Mamakhel, C. Tyrsted, E. D. Bøjesen, P. Hald and B. B. Iversen, *Cryst. Growth Des.*, 2013, **13**, 4730.
- 32 A. Navrotsky, *Geochem. Trans.*, 2003, **4**, 34.
- 33 H. Zhang, B. Chen, J. F. Banfield and G. A. Waychunas, *Phys. Rev. B*, 2008, **78**, 214106.
- 34 H. Zhang and J. F. Banfield, *J. Phys. Chem. B*, 2000, **104**, 3481.
- 35 H. Zhang and J. F. Banfield, *J. Mater. Chem.*, 1998, **8**, 2073.
- 36 A. A. Gribb and J. F. Banfield, *Am. Mineral.*, 1997, **82**, 717.
- 37 D. A. H. Hanaor and C. C. Sorrell, *J. Mater. Sci.*, 2011, **46**, 855.
- 38 Y. Wu, H.-M. Liu, B.-Q. Xu, Z.-L. Zhang and D.-S. Su, *Inorg. Chem.*, 2007, **46**, 5093.
- 39 S. J. Kim, S. D. Park, Y. H. Jeong and S. Park, *J. Am. Ceram. Soc.*, 1999, **82**, 927.
- 40 J.-L. Mi, C. Clausen, M. Bremholm, N. Lock, K. M. Ø. Jensen, M. Christensen and B. B. Iversen, *Cryst. Growth Des.*, 2012, **12**, 6092.
- 41 D. Reyes-Coronado, G. Rodríguez-Gattorno, M. E. Espinosa-Pesqueira, C. Cab, R. d. Coss and G. Oskam, *Nanotechnology*, 2008, **19**, 145605.
- 42 H. Cölfen and S. Mann, *Angew. Chem., Int. Ed.*, 2003, **42**, 2350.
- 43 L. X. Chen, T. Rajh, Z. Wang and M. C. Thurnauer, *J. Phys. Chem. B*, 1997, **101**, 10688.
- 44 P. J. Skrdla, *J. Phys. Chem. A*, 2011, **115**, 6413.
- 45 V. Martis, S. Nikitenko, S. Sen, G. Sankar, W. van Beek, Y. Filinchuk, I. Snigireva and W. Bras, *Cryst. Growth Des.*, 2011, **11**.
- 46 N. Kruse and S. Chenakin, *Applied Catalysis A: General*, 2011, **391**.
- 47 G. S. Li, L. P. Li, J. Boerio-Goates and B. F. Woodfield, *J. Mater. Res.*, 2003, **18**, 2664.
- 48 R. Tauler, *Chemom. Intell. Lab. Syst.*, 1995, **30**, 133.
- 49 J. Jaumot, R. Gargallo, A. de Juan and R. Tauler, *Chemom. Intell. Lab. Syst.*, 2005, **76**, 101.
- 50 H. W. P. Carvalho, S. H. Pulcinelli, C. V. Santilli, F. Leroux, F. Meneau and V. Briois, *Chem. Mater.*, 2013, **25**, 2855.
- 51 M. Staniuk, O. Hirsch, N. Kränzlin, R. Böhlen, W. van Beek, P. M. Abdala and D. Koziej, *Chem. Mater.*, 2014, **26**, 2086.
- 52 V. V. Sraibonyan, A. L. Bugaev, V. V. Pryadchenko, L. A. Avakyan, J. A. van Bokhoven and L. A. Bugaev, *J. Phys. Chem. Solids*, 2014, **75**, 470.
- 53 A. I. Frenkel, C. W. Hills and R. G. Nuzzo, *J. Phys. Chem. B*, 2001, **105**, 12689.
- 54 T. Yao, Z. H. Sun, Y. Y. Li, Z. Y. Pan, H. Wei, Y. Xie, M. Nomura, Y. Niwa, W. S. Yan, Z. Y. Wu, Y. Jiang, Q. H. Liu and S. Q. Wei, *J. Am. Chem. Soc.*, 2010, **132**, 7696.
- 55 K. M. Ø. Jensen, M. Christensen, P. Juhas, C. Tyrsted, E. D. Bøjesen, N. Lock, S. J. L. Billinge and B. B. Iversen, *J. Am. Chem. Soc.*, 2012, **134**, 6785.
- 56 G. V. Jensen, M. Bremholm, N. Lock, G. R. Deen, T. R. Jensen, B. B. Iversen, M. Niederberger, J. S. Pedersen and H. Birkedal, *Chem. Mater.*, 2010, **22**, 6044.
- 57 D. Gebauer, M. Kellermeier, J. D. Gale, L. Bergstrom and H. Colfen, *Chem. Soc. Rev.*, 2014, **43**, 2348.

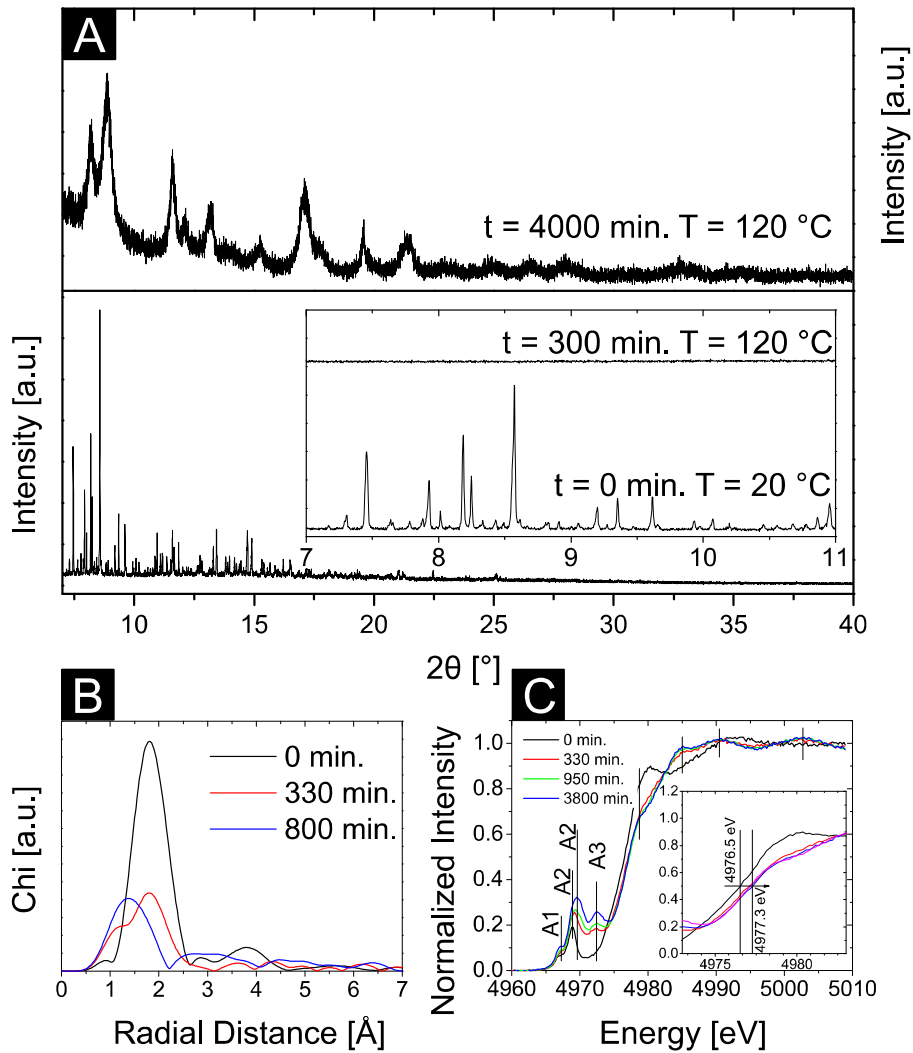


**Figure 1.** A. PXRD patterns, B. Fourier transform of the EXAFS and C. XANES spectra revealing the initial dissolution of the monoclinic  $\text{Ti}(\text{OH})_x\text{Cl}_{4-x}$  crystal phase upon heating the reaction solution to 120 °C and the subsequent growth of rutile and anatase  $\text{TiO}_2$ . The insets show the region of interest for the performed in-situ PXRD and XANES measurements.

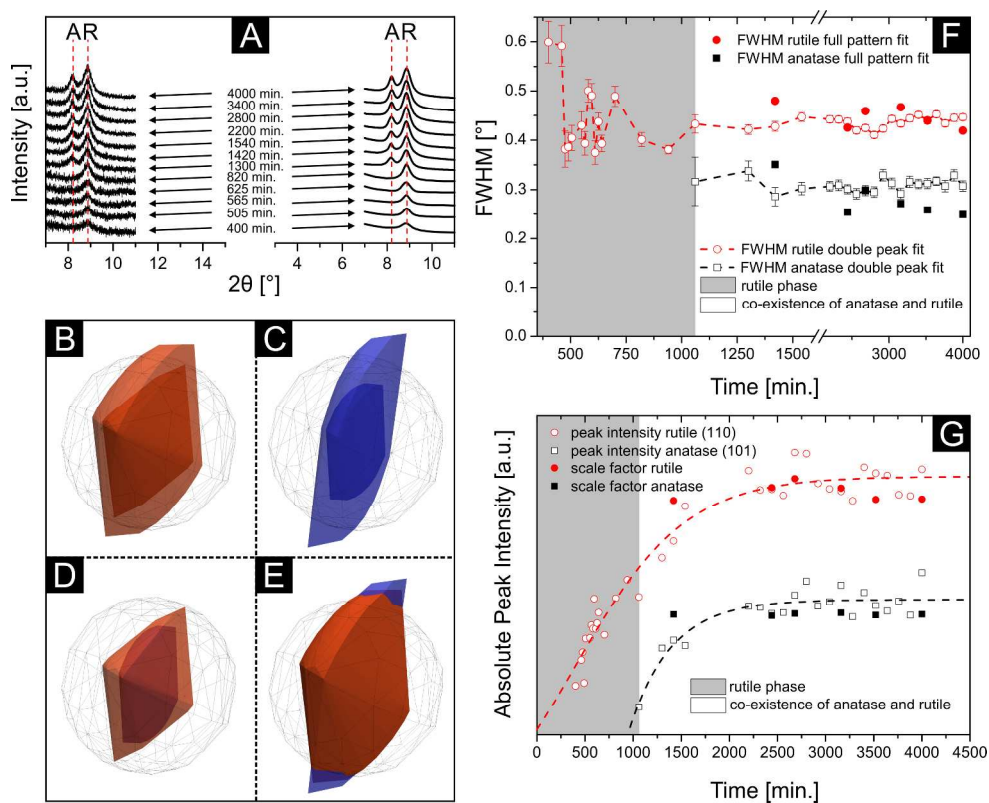


**Figure 2.** A. Anatase and rutile phase evolution starting with the appearance of the first reflection from rutile phase (110) after 400 min of reaction. Left: PXRD pattern as recorded. Right: Fit of the corresponding collected data points. B-E. Graphical representation showing the calculated directional expansions of nanocrystals. B-C. Anatase and rutile nanocrystals after 1420 min of reaction time (smaller inner polyhedron) and after 4000 min (outer translucent polyhedron). D-E. Comparison of anatase (orange) and rutile (blue) after a reaction time of 1420 min and 4000 min, respectively. Superimposed (black lined) is a sphere with diameter  $d = 14$  nm, which represents the critical size for the commonly reported anatase-rutile phase transformation. F. Time evolution of FWHM values and G. peak intensities extracted from (110) reflections in the case of rutile and (101) reflections in the case of anatase. Additionally scale factors output by full pattern fitting of the long range scans are shown.

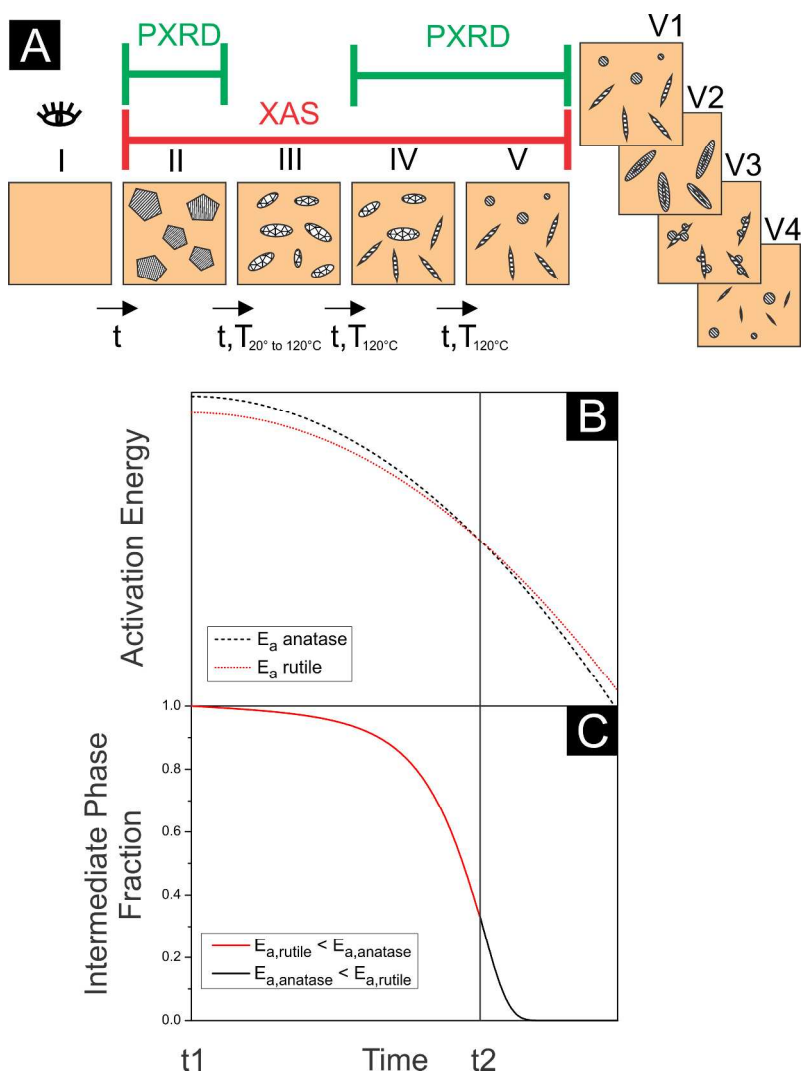


**Figure 3.** A. Different stages representing the final formation of rutile and anatase crystallites. Stage I: Directly after mixing  $\text{TiCl}_4$  with acetone. Stage II: After short time needed to transfer the reaction solution into the experimental cell, a highly crystalline monoclinic  $\text{Ti}(\text{OH})_x\text{Cl}_{4-x}$  phase precipitates. Stage III: The monoclinic crystal phase dissolves upon heating to  $120^\circ \text{C}$  and an intermediate, new Ti containing precursor phase, lacking in long-range periodic order, forms. Stage IV: Onset of rutile crystallization out of the non-crystalline precursor phase. Stage V1 to V4: Hypothetically possible crystallization scenarios for anatase. V1: Anatase crystallizes independently out of the non-crystalline precursor phase. V2: The surface of the rutile crystals undergoes phase transformation to anatase proceeding towards the core of the particles. V3: Anatase heterogeneously nucleates on the rutile crystals' surface and grows. V4: Rutile dissolves and anatase recrystallizes. B. Hypothetical plot of the time dependent activation energies for rutile ( $E_{a, \text{rutile}}$ ) and anatase ( $E_{a, \text{anatase}}$ ), respectively. C. Assuming both polymorphs nucleate out of the intermediate non-crystalline phase, their phase fraction – time transient is drawn.

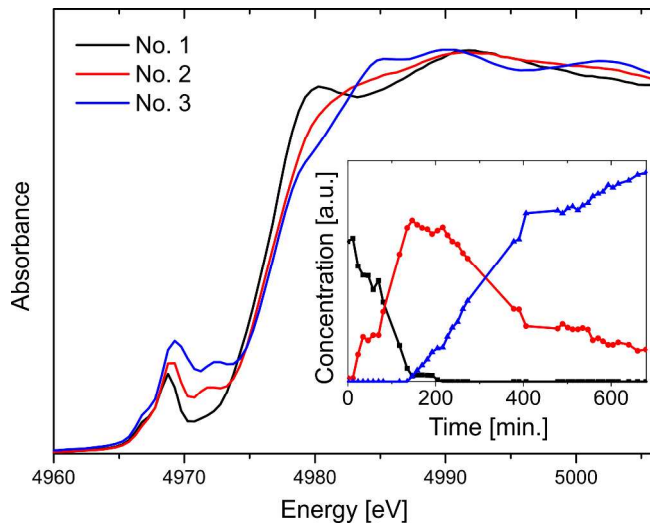


Figure 4. XAS spectra of three Ti components recovered by MCR-ALS analysis. (Inset) Interdependence between the individual components displayed as concentration profiles.